

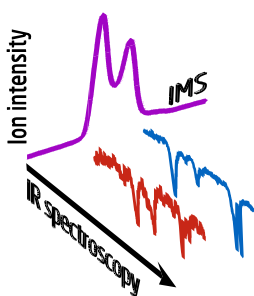
Infrared Spectroscopy of Mobility-Selected H⁺-Gly-Pro-Gly-Gly (GPGG)

Antoine Masson,¹ Michael Z. Kamrath,¹ Marta A. S. Perez,² Matthew S. Glover,³
U. Rothlisberger,² David E. Clemmer,³ Thomas R. Rizzo¹

¹Laboratoire de Chimie Physique Moléculaire, École Polytechnique Fédérale de Lausanne, EPFL SB ISIC LCPM, Station 6, CH-1015, Lausanne, Switzerland

²Laboratoire de Chimie et Biochimie Computationnelles, ISIC, FSB-BCH, École Polytechnique Fédérale de Lausanne (EPFL), CH-1015, Lausanne, Switzerland

³Department of Chemistry, Indiana University, 800 East Kirkwood Avenue, Bloomington, Indiana 47405, USA



Abstract. We report the first results from a new instrument capable of acquiring infrared spectra of mobility-selected ions. This demonstration involves using ion mobility to first separate the protonated peptide Gly-Pro-Gly-Gly (GPGG) into two conformational families with collisional cross-sections of 93.8 and 96.8 Å². After separation, each family is independently analyzed by acquiring the infrared predissociation spectrum of the H₂-tagged molecules. The ion mobility and spectroscopic data combined with density functional theory (DFT) based molecular dynamics simulations confirm the presence of one major conformer per family, which arises from *cis/trans* isomerization about the proline residue. We induce isomerization between the two conformers by using collisional activation in the drift tube and

monitor the evolution of the ion distribution with ion mobility and infrared spectroscopy. While the *cis*-proline species is the preferred gas-phase structure, its relative population is smaller than that of the *trans*-proline species in the initial ion mobility drift distribution. This suggests that a portion of the *trans*-proline ion population is kinetically trapped as a higher energy conformer and may retain structural elements from solution.

Key words: Ion mobility, Infrared spectroscopy, H₂ predissociation, GPGG, Electrospray, Cross-section

Received: 22 January 2015/Revised: 16 April 2015/Accepted: 18 April 2015/Published Online: 20 June 2015

Introduction

Do gas-phase molecules produced by electrospray retain elements of their solution-phase conformations and, if so, under what circumstances [1]? The answers to such questions are essential for determining if and when gas-phase data can be used to explain solution-phase phenomena. However, finding possible links between the gas-phase and solution requires a thorough understanding of the interactions that preserve solution structures in the absence of solvent. These interactions are characterized using several technologies, including mass spectrometry, ion mobility, and vibrational spectroscopy.

Antoine Masson and Michael Z. Kamrath contributed equally to this work.

Electronic supplementary material The online version of this article (doi:10.1007/s13361-015-1172-4) contains supplementary material, which is available to authorized users.

Correspondence to: Thomas R. Rizzo; e-mail: thomas.rizzo@epfl.ch

Of the three technologies mentioned above, mass spectrometry probably provides the most general structural information. It allows one to identify a selected species in the gas phase by its mass and determine the stoichiometry of any noncovalently bound complexes involving that species. Noncovalent complexes have been observed for a variety of protein–protein [2–8] and protein–ligand [9, 4, 10, 11] adducts but are especially revealing in the case of specific heterogeneous multimers [4, 10, 12, 13], which are known to exist in the condensed phase. Unfortunately, mass spectrometry alone cannot tell us how the geometry of such systems might evolve as they transition to the gas phase.

Ion mobility provides complementary information to mass spectrometry in allowing one to separate structures extracted from solution on the basis of their shape (i.e., collisional cross-section) and hence can be used to separate different conformational states. Many systems adopt a variety of structures in the gas phase, some of which may retain memory of their solution-phase conformations whereas others clearly isomerize to

that polar solvents differentially stabilize one structure, whereas the gas-phase environment stabilizes another. These findings are also supported by theoretical calculations.

Experimental

A schematic of the new instrument, which combines an ion mobility drift tube [34] with a cold ion trap [24, 35] and a time-of-flight (TOF) mass spectrometer, is shown in Figure 2. Ions are produced using electrospray ionization and traverse the drift tube in a time that is proportional to their collisional cross-section [36]. The ions then enter an ion trap cooled to ~ 10 K, where they are stored, cooled by collisions with hydrogen, and tagged with weakly bound H₂. Once tagged, the ions are interrogated with an infrared laser, which evaporates H₂ upon resonant photon absorption. This absorption is then detected by monitoring the change in population of the tagged species in a time-of-flight mass spectrometer.

Ion Mobility

The ion mobility drift tube was developed by Clemmer and coworkers [34, 37] and integrated into this instrument without modification. Ions are produced by a homemade electrospray ionization source and collected in a Smith-type ion funnel [38]. These ions are released in discrete packets at a repetition rate of 10 Hz into a 2-m long drift tube, which is filled with helium to a pressure of 3 mbar. A DC voltage gradient of 10–12 V/cm is maintained across the length of the drift tube except in the three ion funnels, located at the source, in the middle, and at the end of the drift tube, where the gradient increases to ~ 15 V/cm. These funnels operate at frequencies of 500–600 kHz and rf voltages of 30–200 V peak-to-peak. Ion mobility drift spectra are recorded at the end of the drift tube using a channeltron detector, and the mobility measurements are calibrated using

bradykinin [M+3H⁺] [18]. When the channeltron is turned off, however, the ions are free to continue through an octopole ion guide and into the cold ion trap for spectroscopic analysis.

The drift tube can be operated as either a single IMS separation stage or as a dual IMS-IMS tandem instrument [34]. In the latter case, an ion gate located at the entrance of the second ion funnel is used to select species having a particular collisional cross-section. In this way, one can monitor the evolution of the selected species as it traverses the second half of the drift tube. There also exists an activation zone at the end of the second funnel where selected species can be collisionally activated before IMS analysis in the second stage of the drift tube. This region consists of two electrodes separated by 3 mm with a voltage drop that can be manipulated independently from the rest of the drift tube, allowing us to change the collision energy in this region in a controlled way. Bieske and coworkers measure visible absorption spectra of ions using a similar IMS-activation-IMS technique by relating photo-induced changes in collisional cross-section to visible light absorption [39–43].

Cold Planar Ion Trap Design

The cold ion trap design was inspired by that published by Wester and coworkers [44] and further developed by Lorenz et al. [35, 45]. The exact geometry used here is similar to that outlined by Lorenz et al. [35]; the primary difference is that the electrodes and electrical connections have been integrated onto a printed circuit board (PCB) to facilitate construction and assembly. The PCBs (shown in the inset of Figure 2) consist of 4 DC electrodes around the perimeter and (32) 1 mm rf electrodes with 1 mm separation, where neighboring electrodes are 180 degrees out of phase. Two PCBs (denoted B and D) are mounted onto an OFHC spacer in direct contact with the second stage of a Sumitomo cryo-cooler (model: RDK-408E2; Darmstadt, Germany) to create the ion trap, while two

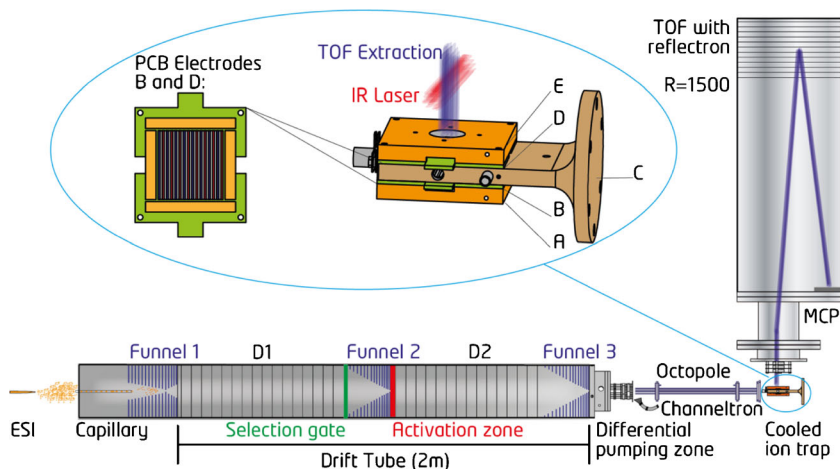


Figure 2. Schematic diagram of the IMS-IR-TOF instrument. Ions are generated with electrospray ionization and separated according to their collisional cross-sections as they traverse the 2-m ion mobility drift tube. The ions are then collected in the cold ion trap where they are collisionally cooled and tagged with H₂ molecules for subsequent spectroscopic analysis. The inset shows a detailed view of the cold ion trap, which consists of two printed circuit boards as described in the text

additional pulsed DC electrodes (denoted A and E) are placed on the top and bottom of the “sandwich” to create a Wiley-McLaren type TOF extraction region [46].

During a trapping cycle, the rf electrodes of B and D oscillate at 2.8 MHz with an amplitude of 500 V_{pp}, whereas electrodes A and E float at a defined DC potential near earth ground. As ions enter the trap, a pulse of H₂ gas, injected by a Parker Series 9 valve, collides with the ions and cools them to a final temperature near that of the trap. The average pressure in the trap chamber is typically 1×10⁻⁵ mbar, which is maintained by a turbomolecular pump with a rated pumping speed of 555 l/s for H₂. We maximize the buffer gas density needed for efficient trapping by limiting the total trap conductance to ~16 l/s at 10 K. The temperature of the trap assembly is maintained at 10 K through the use of a Lake Shore 350 PID controller and cartridge heater and is protected from blackbody radiation by an aluminum heat shield in contact with the first stage of the cryo-cooler. To initiate TOF mass analysis, the oscillating rf voltage is turned off, and electrodes A, B, D, and E are all pulsed to high voltage, ejecting the ions from the trap with translational energies of 3 keV. The TOF drift tube is 1 m long and contains ion optics as well as a 2-stage reflectron from Jordan TOF Inc. (Grass Valley, CA, USA). The M/ΔM mass resolution is typically 1500 at a mass of 287 Da when operating the experiment at 10 Hz.

Infrared Spectroscopy

We acquire infrared spectra through H₂ predissociation as first demonstrated by Okumura et al. [47–49] and later generalized by Johnson [50]. In this process, H₂ adducts are formed with the molecule of interest in the planar ion trap through three-body collisions involving the cold ions and H₂ molecules. The H₂-tagged molecules are then extracted from the trap and intersected with a tunable infrared OPO 2 μs after extraction. Resonant absorption with subsequent intramolecular vibrational redistribution leads to photo-evaporation of H₂, which has a typical binding energy of 370–600 cm⁻¹ [50–52]. This is detected as a dip in the H⁺GPGG · H₂ signal in the time-of-flight analysis. We record the total H⁺GPGG · H₂ ion signal as a function of the IR wavenumber to measure infrared spectra.

Infrared radiation is provided by a Laservision IR OPO pumped by a Nd:YAG laser operating at 10 Hz. The infrared wavenumber is scanned at a rate of 0.06 cm⁻¹/s from 3200 to 3600 cm⁻¹, where typical powers range between 15 and 17 mJ/pulse. The laser is synchronized with the trapping cycle through the use of a BNC pulse generator, while LabView is used for all data collection.

Sample Preparation

We purchased Gly-Pro-Gly-Gly from Bachem Inc. (Bubendorf, Switzerland) and used it without further purification. The ESI samples were prepared by making a 2×10⁻⁴ M solution of GPGG in methanol, water, and acetic acid (50:50:0.5).

Computational Methods

We performed full quantum (DFT) calculations to determine the 3D structures of the possible H⁺GPGG conformers. Initially, 10 H⁺GPGG conformers, (7 *L-trans*-Pro and 3 *L-cis*-Pro) were created as starting structures using the backbone coordinates of different randomly chosen fragments from the protein data bank that contain Pro at position 2. For each initial structure, simulated annealing ab initio molecular dynamics (SA-AIMD) runs were performed with the Terachem program [53–55] using the functional B3LYP [56–58] and a 6-31G basis [59]. During these SA-AIMD runs, the conformers were heated to high temperatures to accelerate phase-space sampling and then slowly cooled to 6 K. For a more comprehensive sampling, different maximal heating temperatures (between 900 and 1100 K) and different cooling rates (total simulation times between 40 and 100 ps) were applied. At higher temperatures, (>1200 K) spontaneous enantiomerization from *L*-Pro to *D*-Pro occurred. In total, 80 conformers were obtained from the SA-AIMD runs (including the final cooling product and different candidate structures from fast quenches at finite temperature). For each conformer, the geometry was optimized at the DFT B3LYP//6-31G(d,p) level using Gaussian09 v D.01 [60], and the orientationally-averaged geometric cross-section was calculated using the Trajectory Method (TM) with the Mobcal software [61, 62] through consideration of only Lennard-Jones interactions. Finally, the five lowest-energy *L-cis*-Pro and *L-trans*-Pro conformers obtained were re-optimized and the respective harmonic vibrational frequencies calculated with B3LYP and a larger basis set 6-311++G(d,p) using Gaussian09 v D.01 [60] with tight convergence criteria and ultrafine grid. All the computed energies were zero-point corrected, and harmonic vibrational frequencies were rescaled with a constant factor of 0.955—a value chosen to maximize the agreement between theory and experiment in the N–H and OH stretch regions for the 10 lowest energy conformations. The correspondence between theoretical and experimental IR spectra for the lowest energy conformers (Supplementary Table S1) and the good agreement of average collisional cross-sections allows for a reliable identification of the 3D structures of the experimentally detected species.

Results and Discussion

The ion mobility drift distribution for H⁺GPGG is shown in Figure 3b. Two peaks, labeled A and B, are present with collisional cross-sections of 93.8 and 96.8 Å², respectively. There are additional features in the drift distribution that we identify as multimers using mass spectrometry; however, in this report we focus our attention on the H⁺GPGG species and eliminate these other species from our analysis using the selection gate in the drift tube. In this way, we isolate the two features shown in Figure 3b, the cross-sections of which are in excellent agreement with the values 93.2 and 96.4 Å² published previously [32].

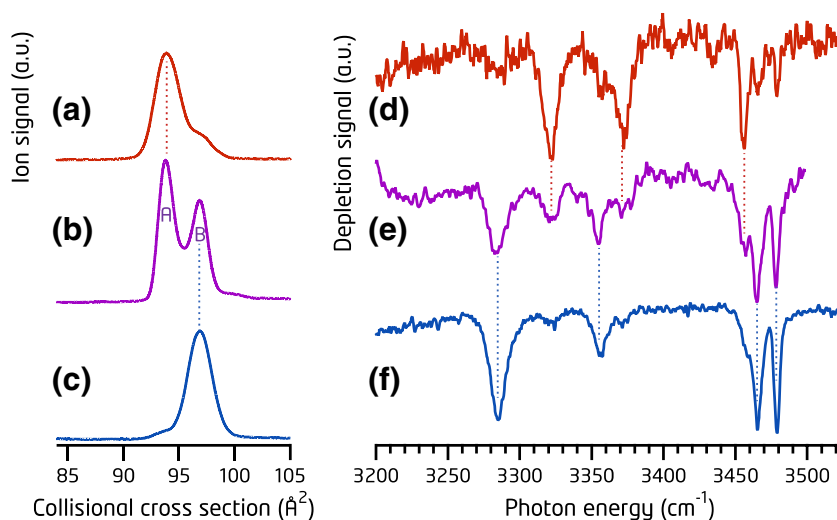


Figure 3. Ion mobility cross-section distribution for H⁺GPGG in **(b)** with the corresponding H₂ predissociation spectrum in **(e)**. By mobility selecting ions having collisional cross-sections of **(a)** 93.8 Å² and **(c)** 96.8 Å², we obtain H₂ predissociation spectra shown in **(d)** and **(f)**, respectively. This indicates the presence of at least two conformers as described in the text

Infrared Spectroscopy of the Mobility Selected Ions

Having reproduced the known cross-section distribution of H⁺GPGG, we used vibrational spectroscopy to elucidate the structures of these species. In doing this, the key question we were trying to answer was, “How many distinct conformations are responsible for producing the two peaks in the ion mobility drift spectrum?” We address this question by first presenting in Figure 3e the infrared spectrum acquired by loading all H⁺GPGG ions (both A and B) into the cold ion trap. Since H⁺GPGG has five N–H oscillators as shown in Figure 1, one may expect to observe up to five bands per conformer in the N–H stretching region of the infrared spectrum. However, the IR spectrum in Figure 3e contains as many as seven prominent bands. The fact that there are more absorption bands in the spectrum than oscillators in the molecule is one indication that multiple conformers are present.

In order to confirm that this is the case, we use the ion gate to load ions contained within either peak A or peak B into the ion trap. We begin by isolating peak A via its ion mobility, as shown in Figure 3a, and allow it to continue to the ion trap. The corresponding infrared spectrum we obtain contains three prominent bands, shown in Figure 3d, as opposed to the seven that appear in the absence of ion mobility selection (Figure 3e). The positions of these three bands are consistent with a subset of those in the non-mobility-selected spectrum. There are traces of the other four bands; however, their intensities have been greatly reduced. Of the three strong N–H stretching bands we observe, two appear at 3322 and 3372 cm⁻¹, whereas the third appears significantly higher in energy, at 3456 cm⁻¹.

In a similar manner, we use the selection gate to isolate peak B in the cross-section distribution (Figure 3c) and obtain the infrared spectrum shown in Figure 3f. This time we observe four bands, the positions of which are clearly different than those observed when selecting peak A, signaling that the local

environment of these oscillators within the molecule has changed. An intense band appears at 3284 cm⁻¹ in addition to a much weaker transition at 3355 cm⁻¹. The other two bands appear higher in energy 3465 and 3478 cm⁻¹, respectively. The fact that the infrared spectrum changes upon selecting different peaks in the ion mobility drift-time distribution indicates that the two features in the cross-section distribution arise from two distinct conformational families of H⁺GPGG. We refer to the conformations associated with peak A and peak B as conformers A and B, respectively. There are other weak transitions in the spectra (e.g., at 3434 cm⁻¹ in Figure 3d), which may signal the presence of conformational heterogeneity within these two populations, and these will be addressed later. While in principle, the infrared spectra displayed in Figure 3 could also be affected by gain from H⁺GPGG·2H₂ complexes that photodissociate to form the H⁺GPGG·H₂, this would be at most a minor effect, since the population of H⁺GPGG·2H₂ is typically only 15% of the singly tagged species (Supplementary Figure S1). Since we know that the strongest N–H stretching transitions result in a ~20% population depletion of the tagged species, we estimate that this effect could translate to a 3% fluctuation in the population of H⁺GPGG·H₂, which is below our current signal-to-noise level.

The band patterns shown in Figure 3d and f reveal qualitative information about the hydrogen bonding patterns in the molecules. The N–H stretches that give rise to bands above ~3380 cm⁻¹ are typically considered to be “free” oscillators [63], that is, they do not participate in noncovalent interactions such as hydrogen bonds. In contrast, the vibrations that occur below ~3380 cm⁻¹ likely participate in H-bonding interactions, which shift their frequencies to the red. In order to extract as much information as possible from the measured spectra, we isolate the transitions that arise from conformer A by first scaling the spectrum of conformer B to the peak at 3284 cm⁻¹,

and then subtracting it from the spectrum of A. We do this because there is clearly contamination from conformer B in the spectrum of A. The result of this subtraction is a much cleaner spectrum, shown in Figure 4a, which clearly indicates the presence of only a single free N–H. Furthermore, the absence of a free OH stretching band in the region from 3500 to 3600 cm⁻¹ implies that the carboxylic acid OH participates in a hydrogen bond. The spectrum for conformer B, on the other hand, reveals a distinctly different hydrogen bonding pattern, where the OH (appearing at 3572 cm⁻¹) and two N–H oscillators are free (see Figure 4b). This information is especially useful in determining the structures of a molecule the size of H⁺GPGG, where the total number of potential hydrogen bonding partners is limited.

We now have two experimentally determined criteria that any calculated structures for conformers A and B must meet. The first is that they must match the experimental cross-sections of 93.8 and 96.8 Å² for conformers A and B, respectively. The second criterion is that the structure of conformer A must have one free N–H and one hydrogen bonded OH, while the structure for conformer B must have two free N–H's and a free OH.

Theoretical Analysis of the Experimental Infrared Spectra

The lowest energy calculated structures are shown in Figure 4c and d, with their corresponding vibrational spectra (indicated as sticks) in Figure 4a and b. The calculations reveal that conformer B (Figure 4d) is the lowest energy structure and

corresponds to a geometry having a *cis*-Pro configuration. The spectrum of this species (Figure 4b) exhibits two free N–H stretches, which correspond to those on Gly³ and Gly⁴. The OH remains free because the carbonyl of Gly⁴ forms a strong hydrogen bond with one of the N-terminal ammonium N–H's, thus orienting the O–H to the outside. In this structure, all three ammonium N–H's are involved to various degrees in hydrogen bonding interactions, which leads to a red shift in the NH₃ antisymmetric stretch band, which we observe at 3284 cm⁻¹.

Interestingly, the calculations reveal two classes of *cis*-Pro conformers arising from rotation about the ^αC–C bond of the proline residue—the first orients the proline C=O toward the protonated amine and is lower in energy, while the second orients it away from the protonated amine. The orientation of this bond influences the positions of the ammonium N–H stretch bands. Comparison of the results of our calculated structures and spectra with the experimental data suggest that both types of species likely exist in our experiment. The dominant and more stable class of conformers is that with its proline C=O oriented toward the protonated amine, as shown in Figure 4d. However, the small peak at 3355 cm⁻¹ suggests the presence of a minor conformer with its proline C=O oriented away from the protonated amine (see Supplementary Figure S2), which is 5.7 kJ mol⁻¹ higher in energy. Both *cis*-Pro conformers can be populated at the drift tube temperature of 300 K, and a simple Boltzmann calculation reveals that the minor conformer should make up 10% of the population of the major *cis*-Pro conformer.

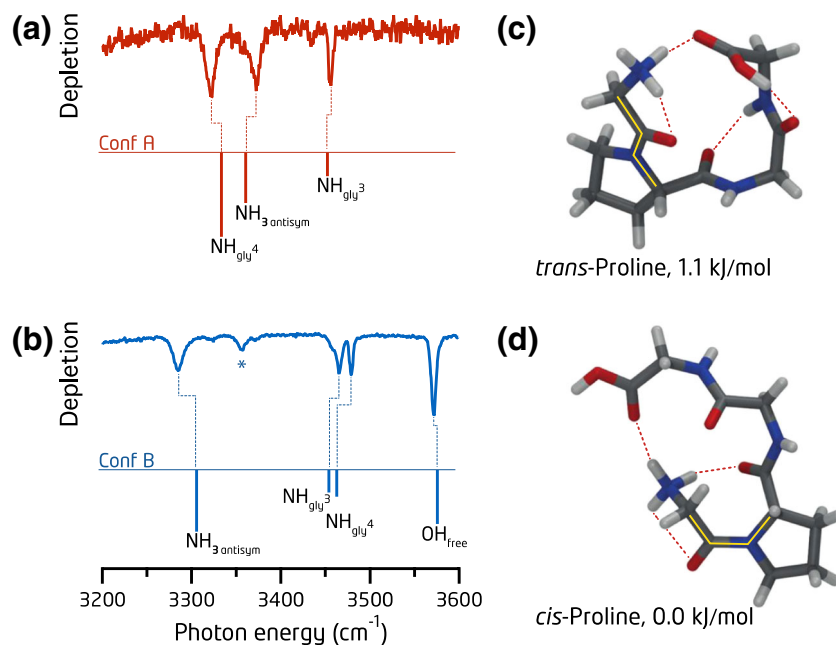


Figure 4. Infrared H₂ predissociation spectra of H⁺GPGG·H₂ for (a) conformer A, and (b) conformer B. The experimental spectrum in (a) was prepared by subtracting contributions from conformer B as described in the text. Geometry optimization and vibrational frequency calculations are performed at the B3LYP/6-311++G(d,p) level of theory and reveal the presence of both (c) *trans* and (d) *cis* structures. Calculated spectra are shown below the respective experimental spectra for comparison. The asterisk denotes a peak originating from a minor conformer shown in the Supplementary Material (Supplementary Figure S2)

We now turn our attention to conformer A, shown in Figure 4c, which is the second lowest energy conformer overall (1.1 kJ/mol above conformer B) and the lowest energy *trans*-Pro species recovered in our theoretical search. The measured spectrum (Figure 4a) constrains a valid structure for this conformer to have only one free N–H stretch. Indeed, the calculated structure shown in Figure 4c meets this criterion, with a free Gly³ N–H stretch predicted at 3452 cm⁻¹. Interestingly, the position of the antisymmetric NH₃-Gly¹ vibration at 3360 cm⁻¹ is shifted to the blue relative to its position in the *cis*-Pro species, since in the latter, all three ammonium N–H oscillators form hydrogen bonds. In the *trans*-Pro species, however, only two form hydrogen bonds, which shift the NH₃-Gly¹ vibrations to the blue. The substantial redshift of the Gly⁴ N–H stretch band in conformer A at 3334 cm⁻¹ relative to that in conformer B can be explained by the participation of both the Gly⁴ N–H and carbonyl oxygen in forming hydrogen bonds. Conformer A also exhibits a hydrogen bonded O–H with the carbonyl group of Gly³, shifting the O–H vibration to 3018 cm⁻¹, which is outside of our experimental observation window.

We should note that although ammonium generally has three N–H stretching vibrations (two antisymmetric and one symmetric), we only observe one of these in our experiment for both the *trans*-Pro and *cis*-Pro species. The other two vibrations fall outside our observation region, at 3125 and 3017 cm⁻¹ for conformer A and at 3147 and 3106 cm⁻¹ for conformer B. A strong red shift in the bands associated with the protonated amine is consistent with a number of previous experimental studies [51, 52, 64].

Comparison of Experimental Cross-Sections and Calculated Lowest-Energy Geometries

In addition to calculating vibrational frequencies, we performed collisional cross-section calculations to further validate the structures proposed above. These yielded cross-section values of 94.8 Å² for the *trans*-Pro geometry and 99.2 Å² for the *cis*-Pro geometry, compared with the measured values of 93.8 and 96.8 Å², respectively. These calculated values agree with experiment to within 1.1% and 2.5% for the *trans*-Pro and *cis*-Pro geometries, which is within the typical error of 3% that is commonly observed when calculating collisional cross-sections [62, 65].

In combining ion mobility and vibrational spectroscopy for the study of larger molecules, one could use the experimentally determined cross-section as a filter to select which structures generated by force-field calculations should be optimized at the DFT level, greatly reducing the computational demands. These structures would then be validated through comparison of calculated vibrational frequencies with the measured infrared spectra.

Collision-Induced Isomerization Between Conformers

Up to this point, we have shown that cold ion spectroscopy can be used to measure the infrared signatures of molecules first

separated with ion mobility. This combination of tools provides both collisional cross-sections as well as internal hydrogen-bonding information for the selected species, which in turn leads to structural assignments when combined with theoretical calculations. With the two major conformations of *trans*-Pro and *cis*-Pro assigned, we now turn our attention to a second question: “Are either the *trans*-Pro or *cis*-Pro conformers kinetically trapped?” If so, it should be possible to introduce energy into the molecules and induce isomerization between the two conformers. It is important to answer this question because kinetically trapped species may retain much of their solution phase conformation and, thus, the IMS-IR technique may provide information on the structure of species in solution.

We select the *trans*-Pro conformer and employ collisional activation as a means of introducing energy into the molecules. We energize the ions in the “activation zone,” shown in Figure 2, once they have traversed the first half of the drift tube. Figure 5 displays the results of this experiment. As we increase the activation voltage, peak A decreases in intensity while a new peak with the same cross-section as the *cis*-Pro configuration grows in. We refer to this new feature as peak B', since we do not yet know whether this new feature directly corresponds to the *cis*-Pro conformation we have already measured; all we can say is that it has the same cross-section as the *cis*-Pro species. We observe that peak B' grows to 50% of the intensity of peak A when activating with 10 V. As we continue to increase the collision energy, peak A progressively becomes smaller while peak B' grows in. However, once we pass 50 V in

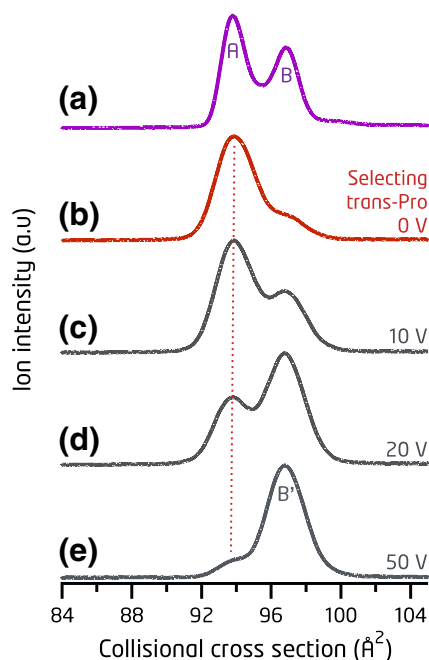


Figure 5. Cross-section distribution of (a) H⁺GPGG and (b) a selection where peak A has been isolated. Traces (c)–(e) show that population is transferred from peak A to peak B' upon collisional activation

the activation region, the cross-section distribution ceases to change, with most of the population having been transferred from peak A to peak B'. Because further activation has no further effect on the peak intensities and, hence, the conformer populations, it appears that we create a “quasi-equilibrium” distribution of conformers. Pierson et al. reported similar behavior for bradykinin [M+3H]³⁺ when energizing the ions in IMS-IMS experiments [18].

We can identify the structure that gives rise to peak B' by using infrared spectroscopy. Figure 6a shows once again the infrared spectrum we obtained when selecting the *trans*-Pro configuration (conformer A) and 6d shows that for the *cis*-Pro configuration (conformer B). The infrared spectrum of the *trans*-Pro species has three prominent bands, and as the activation voltage increases to 20 V, these bands are joined by four others, as shown in Figure 6b. One can see that these four new peaks are identical to those associated with the *cis*-Pro species. This means that a certain portion of the population that began as *trans*-Pro has now isomerized to *cis*-Pro. It is difficult to calculate the exact makeup of the conformer distribution because we do not know the relative absorption cross-sections. However, it is clear that by increasing the activation voltage, we continue to drive the conformer distribution toward the *cis*-Pro configuration. When activating with 50 V, the bands associated with *trans*-Pro have nearly disappeared, while those associated with *cis*-Pro dominate. If we continue activating beyond 50 V, the relative peak intensities do not appreciably change from those depicted in Figure 6c. This is consistent with the ion mobility data presented in Figure 5 and again suggests

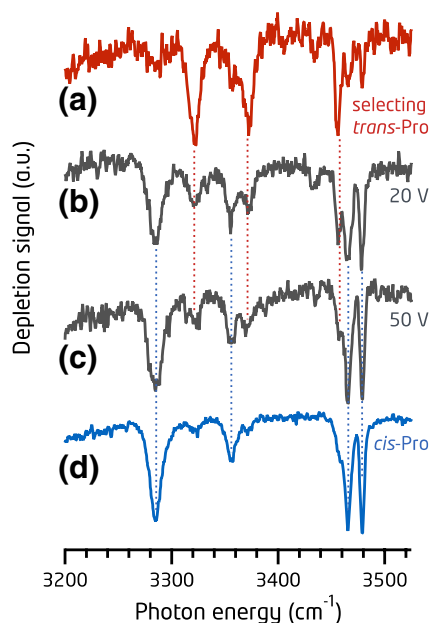


Figure 6. Infrared predissociation spectra of H⁺GPGG-H₂ acquired while isolating peak A in the ion mobility drift distribution. Trace (a) displays the spectrum acquired for the *trans*-Pro species. Traces (b) and (c) show how the spectrum evolves as the activation energy is increased. The spectrum for the *cis*-Pro species is provided in (d) for comparison

that we cannot fully convert the original *trans*-Pro population to *cis*-Pro configuration. The only change we observe beyond this point is that the signal-to-noise ratio degrades, likely because the ion transmission decreases as the molecules begin to fragment. We also perform the opposite experiment, selecting *cis*-Pro molecules and then activating them via collisions. This experiment generates consistent results and confirms that it is possible to interconvert between conformers as discussed in detail in the supplementary material (see Supplementary Figures S3 and S4).

The Case for Quasi-Equilibrium and Kinetic Trapping from Solution

As demonstrated in the data of Figures 5, 6 and Supplementary Figures S3, S4, collisional activation produces the same conformer distribution regardless of the distribution with which we begin. With ~50 V of activation, both the ion mobility data and infrared spectrum for the two conformers become nearly indistinguishable. This strongly suggests that this distribution represents a quasi-equilibrium in the gas phase. This distribution consists mostly of the *cis*-Pro configuration and a much smaller amount of the *trans*-Pro, implying that the former is more stable. The *trans*-Pro species readily isomerizes to *cis*-Pro when it is energized by collisions; however, under the room temperature conditions of our drift tube, it is still energetically accessible and remains a small portion of the annealed distribution. A similar observation has been made for a variety of other peptidic systems [18, 31] and suggests that the relative conformer populations we measure after annealing reflect the Boltzmann weights of these states at a given temperature. The exact temperature to which the relative populations correspond is not obvious; however, it may reflect that of the drift tube (300 K), but it may also reflect a higher temperature, depending on the rate of cooling in the drift tube and the height of the barriers separating the conformers.

A final question to address is that of the origin of the *trans*-Pro configuration, which has a substantial population if we do not anneal the gas-phase conformer distribution. It is clear that the majority of the population cannot originate in the gas phase and, thus, there remain only two alternatives: it either reflects the population of this conformer in solution, which survives the electrospray process, or the conditions in the electrospray droplets. A possible way to address this question would be to change the solution conditions, for example by changing the solvent or concentration of the solute and measuring the *cis*-Pro to *trans*-Pro ratio in the ion mobility spectra [19, 66].

Another way to determine the origin of the *trans*-Pro conformation is to compare our results to solution-phase studies. The GPGG molecule has been studied in solution using NMR spectroscopy, and the *trans*-Pro species was found to be more stable in D₂O by 4.5 kJ mol⁻¹ [33]. This is consistent with the nonactivated ion mobility drift distribution we measure, where the *trans*-Pro species is clearly more abundant. This implies that the ion mobility drift distribution samples states that

originate in solution. The relative stabilities switch in the gas phase; however, as demonstrated by both our calculations and experiments, this may indicate that the *trans*-Pro conformation is preferentially stabilized by interactions with polar solvents. This would explain why in the absence of solvent it is so easy to induce *cis*-to-*trans* isomerization. This could perhaps be further explored by performing calculations with solvent or by running NMR experiments at low pH to favor formation of the protonated species. In this way, one could measure the *cis/trans* populations for the protonated species in solution directly and compare the results with our experiment.

Conclusions

In this paper, we have presented first results from a new instrument that combines ion mobility, cold ion spectroscopy, and mass spectrometry. As an initial test, we reproduced the two-feature ion mobility distribution of the small peptide H⁺GPGG reported in an earlier study [32] and analyzed both features with infrared spectroscopy. The vibrational spectra and collisional cross-sections were compared with those obtained in our theoretical analysis. We found that the two features isolated with ion mobility arise from two well-defined classes of conformers originating from *cis-trans* isomerization about the proline residue. We then isolated each of the conformers (referred to as *trans*-Pro and *cis*-Pro configurations) with ion mobility, used collisional activation to induce isomerization, and monitored the conformer distribution with infrared spectroscopy. We observed interconversion between the two conformers when selecting either the *trans*-Pro or *cis*-Pro species; however, the *cis*-Pro configuration seems to be favored from a thermodynamic point of view. Interestingly, after subjecting either conformer to >50 V activation, the conformer distribution strongly favors *cis*-Pro and approaches a steady state in which increasing the activation energy further does not appreciably change the relative ratio of the two species. The evolution of the original ion distribution to this gas-phase quasi-equilibrium implies that this technique may allow us to sample states that come directly from solution.

This multidimensional approach to molecular structural characterization provides several benefits over using either one of the techniques alone. From a spectroscopic point of view, the addition of ion mobility provides a conformational filter that can simplify the vibrational spectra. In addition, it provides experimentally determined collisional cross-sections, which can be used to narrow the conformer search space in calculating structures. From an ion mobility standpoint, spectroscopy allows one to recover the vibrational signatures of isolated species, thus providing information that can lead to structural determination. Taken together, this approach could be used to identify kinetically trapped species, which may originate in solution, and to structurally characterize these species. As such, it may provide an additional probe of condensed phase molecules.

Acknowledgments

T.R.R. thanks the EPFL and the Swiss National Science Foundation under grant numbers 200020_152804 for their generous support of this work. The IMS instrumentation was developed in part with support from the NIH (1RC1GM090797-01). U.R. thanks EPFL for computing resources.

References

- Hoaglund-Hyzer, C.S., Counterman, A.E., Clemmer, D.E.: Anhydrous protein ions. *Chem. Rev.* **99**, 3037–3080 (1999)
- Ruotolo, B.T., Giles, K., Campuzano, I., Sandercock, A.M., Bateman, R.H., Robinson, C.V.: Evidence for Macromolecular protein rings in the absence of bulk water. *Science* **310**, 1658–1661 (2005)
- Ruotolo, B.T., Robinson, C.V.: Aspects of native proteins are retained in vacuum. *Curr. Opin. Chem. Biol.* **10**, 402–408 (2006)
- Veenstra, T.D.: Electrospray ionization mass spectrometry in the study of biomolecular non-covalent interactions. *Biophys. Chem.* **79**, 63–79 (1999)
- Ethier, M., Lambert, J.P., Vasilescu, J., Figeys, D.: Analysis of protein interaction networks using mass spectrometry compatible techniques. *Anal. Chim. Acta* **564**, 10–18 (2006)
- Strupat, K., Rogniaux, H., Van Dorsselaer, A., Roth, J., Vogl, T.: Calcium-induced noncovalently linked tetramers of MRP8 and MRP14 are confirmed by electrospray ionization-mass analysis. *J. Am. Soc. Mass Spectrom.* **11**, 780–788 (2000)
- Smits, A.H., Jansen, P., Poser, I., Hyman, A.A., Vermeulen, M.: Stoichiometry of chromatin-associated protein complexes revealed by label-free quantitative mass spectrometry-based proteomics. *Nucleic Acids Res.* **41**(1):e28 (2013)
- Pukala, T.L.: Mass spectrometry for structural biology: determining the composition and architecture of protein complexes. *Aust. J. Chem.* **64**, 681–691 (2011)
- Loo, J.A.: Studying noncovalent protein complexes by electrospray ionization mass spectrometry. *Mass Spectrom. Rev.* **16**, 1–23 (1997)
- Robinson, C.V., Chung, E.W., Kragelund, B.B., Knudsen, J., Aplin, R.T., Poulsen, F.M., Dobson, C.M.: Probing the nature of noncovalent interactions by mass spectrometry. A study of protein-CoA ligand binding and assembly. *J. Am. Chem. Soc.* **118**, 8646–8653 (1996)
- Sobott, F., Robinson, C.V.: Characterising electrosprayed biomolecules using tandem-MS—the noncovalent GroEL chaperonin assembly. *Int. J. Mass Spectrom.* **236**, 25–32 (2004)
- Loo, J.A.: Electrospray ionization mass spectrometry: a technology for studying noncovalent macromolecular complexes. *Int. J. Mass Spectrom.* **200**, 175–186 (2000)
- Sharon, M., Robinson, C.V.: The role of mass spectrometry in structure elucidation of dynamic protein complexes. *Annu. Rev. Biochem.* **76**, 167–193 (2007)
- Wytttenbach, T., Bowers, M.T.: Structural stability from solution to the gas phase: native solution structure of ubiquitin survives analysis in a solvent-free ion mobility–mass spectrometry environment. *J. Phys. Chem. B* **115**, 12266–12275 (2011)
- Pierson, N.A., Clemmer, D.E.: An IMS–IMS threshold method for semi-quantitative determination of activation barriers: interconversion of proline *cis*↔*trans* forms in triply protonated bradykinin. *Int. J. Mass Spectrom.* **377**, 646–654 (2015)
- Koeniger, S.L., Merenbloom, S.I., Sevugarajan, S., Clemmer, D.E.: Transfer of structural elements from compact to extended states in unsolvated ubiquitin. *J. Am. Chem. Soc.* **128**, 11713–11719 (2006)
- Koeniger, S.L., Merenbloom, S.I., Clemmer, D.E.: Evidence for many resolvable structures within conformation types of electrosprayed ubiquitin ions. *J. Phys. Chem. B* **110**, 7017–7021 (2006)
- Pierson, N.A., Valentine, S.J., Clemmer, D.E.: Evidence for a quasi-equilibrium distribution of states for Bradykinin [M + 3H]⁽³⁺⁾ ions in the gas phase. *J. Phys. Chem. B* **114**, 7777–7783 (2010)
- Wytttenbach, T., Pierson, N.A., Clemmer, D.E., Bowers, M.T.: Ion mobility analysis of molecular dynamics. *Annu. Rev. Phys. Chem.* **65**, 175–196 (2014)
- Skinner, O., McLafferty, F., Breuker, K.: How ubiquitin unfolds after transfer into the gas phase. *J. Am. Soc. Mass Spectrom.* **23**, 1011–1014 (2012)

21. Polfer, N.C., Oomens, J.: Vibrational spectroscopy of bare and solvated ionic complexes of biological relevance. *Mass Spectrom. Rev.* **28**, 468–494 (2009)
22. Oomens, J., Sartakov, B.G., Meijer, G., Von Helden, G.: Gas-phase infrared multiple photon dissociation spectroscopy of mass-selected molecular ions. *Int. J. Mass Spectrom.* **254**, 1–19 (2006)
23. Wolk, A.B., Leavitt, C.M., Garand, E., Johnson, M.A.: Cryogenic ion chemistry and spectroscopy. *Acc. Chem. Res.* **47**, 202–210 (2014)
24. Svendsen, A., Lorenz, U.J., Boyarkin, O.V., Rizzo, T.R.: A new tandem mass spectrometer for photofragment spectroscopy of cold, gas-phase molecular ions. *Rev. Sci. Instrum.* **81**(7):073107-1–073107-7 (2010)
25. Goebbert, D.J., Wende, T., Bergmann, R., Meijer, G., Asmis, K.R.: Messenger-tagging electrosprayed ions: vibrational spectroscopy of substrate dianions. *J. Phys. Chem. A* **113**, 5874–5880 (2009)
26. Boyarkin, O.V., Mercier, S.R., Kamariotis, A., Rizzo, T.R.: Electronic spectroscopy of cold, protonated tryptophan and tyrosine. *J. Am. Chem. Soc.* **128**, 2816–2817 (2006)
27. Elliott, B.M., Relph, R.A., Roscioli, J.R., Bopp, J.C., Gardenier, G.H., Guasco, T.L., Johnson, M.A.: Isolating the spectra of cluster ion isomers using Ar-"tag"-mediated IR-IR double resonance within the vibrational manifolds: application to NO(2)(-)center dot H₂O. *J. Chem. Phys.* **129**(9):094303-1–094303-6 (2008)
28. Relph, R.A., Guasco, T.L., Elliott, B.M., Kamrath, M.Z., McCoy, A.B., Steele, R.P., Schofield, D.P., Jordan, K.D., Viggiano, A.A., Ferguson, E.E., Johnson, M.A.: How the shape of an H-bonded network controls proton-coupled water activation in HONO formation. *Science* **327**, 308–312 (2010)
29. Camey, J.R., Zwier, T.S.: The infrared and ultraviolet spectra of individual conformational isomers of biomolecules: tryptamine. *J. Phys. Chem. A* **104**, 8677–8688 (2000)
30. Warnke, S., Baldauf, C., Bowers, M.T., Pagel, K., von Helden, G.: Photodissociation of conformer-selected ubiquitin ions reveals site-specific *cis/trans* isomerization of proline peptide bonds. *J. Am. Chem. Soc.* **136**, 10308–10314 (2014)
31. Papadopoulos, G., Svendsen, A., Boyarkin, O.V., Rizzo, T.R.: Conformational distribution of Bradykinin [bk + 2 H](2+) revealed by cold ion spectroscopy coupled with FAIMS. *J. Am. Soc. Mass Spectrom.* **23**, 1173–1181 (2012)
32. Counterman, A.E., Clemmer, D.E.: *Cis/trans* signatures of proline-containing tryptic peptides in the gas phase. *Anal. Chem.* **74**, 1946–1951 (2002)
33. Aliev, A.E., Bhandal, S., Courtier-Murias, D.: Quantum mechanical and NMR studies of ring puckering and *cis/trans*-rotameric interconversion in prolines and hydroxyprolines. *J. Phys. Chem. A* **113**, 10858–10865 (2009)
34. Koeniger, S.L., Merenbloom, S.I., Valentine, S.J., Jarrold, M.F., Udseth, H.R., Smith, R.D., Clemmer, D.E.: An IMS-IMS analogue of MS-MS. *Anal. Chem.* **78**, 4161–4174 (2006)
35. Lorenz, U.J., Rizzo, T.R.: Planar multipole ion trap/time-of-flight mass spectrometer. *Anal. Chem.* **83**, 7895–7901 (2011)
36. Mason, E.A., McDaniel, E.W.: *Transport Properties of Ions in Gases*. Wiley, New York (1988)
37. Merenbloom, S.I., Koeniger, S.L., Valentine, S.J., Plasencia, M.D., Clemmer, D.E.: IMS-IMS and IMS-IMS-IMS/MS for separating peptide and protein fragment ions. *Anal. Chem.* **78**, 2802–2809 (2006)
38. Tang, K., Shvartsburg, A.A., Lee, H.-N., Prior, D.C., Buschbach, M.A., Li, F., Tolmachev, A.V., Anderson, G.A., Smith, R.D.: High-sensitivity ion mobility spectrometry/mass spectrometry using electrodynamic ion funnel interfaces. *Anal. Chem.* **77**, 3330–3339 (2005)
39. Coughlan, N.J.A., Adamson, B.D., Catani, K.J., Wille, U., Bieske, E.J.: Ion mobility unlocks the photofragmentation mechanism of retinal protonated Schiff base. *J. Phys. Chem. Lett.* **5**, 3195–3199 (2014)
40. Coughlan, N.J.A., Catani, K.J., Adamson, B.D., Wille, U., Bieske, E.J.: Photoisomerization action spectrum of retinal protonated Schiff base in the gas phase. *J. Chem. Phys.* **140**, 164307 (2014)
41. Adamson, B.D., Coughlan, N.J.A., da Silva, G., Bieske, E.J.: Photoisomerization action spectroscopy of the carbocyanine dye DTC⁺ in the gas phase. *J. Phys. Chem. A* **117**, 13319–13325 (2013)
42. Adamson, B.D., Coughlan, N.J.A., Continetti, R.E., Bieske, E.J.: Changing the shape of molecular ions: photoisomerization action spectroscopy in the gas phase. *Phys. Chem. Chem. Phys.* **15**, 9540–9548 (2013)
43. Adamson, B.D., Coughlan, N.J.A., Markworth, P.B., Continetti, R.E., Bieske, E.J.: An ion mobility mass spectrometer for investigating photoisomerization and photodissociation of molecular ions. *Rev. Sci. Instrum.* **85**, 123109 (2014)
44. Debatin, M., Kröner, M., Mikosch, J., Trippel, S., Morrison, N., Reetz-Lamour, M., Woias, P., Wester, R., Weidemüller, M.: Planar multipole ion trap. *Phys. Rev. A* **77**, 033422-1–033422-6 (2008)
45. Marmillod, P., Antonioni, S., Lorenz, U.J.: A radio frequency/high voltage pulse generator for the operation of a planar multipole ion trap/time-of-flight mass spectrometer. *Rev. Sci. Instrum.* **84**, 04470715 (2013)
46. Wiley, W.C., McLaren, I.H.: Time-of-flight mass spectrometer with improved resolution. *Rev. Sci. Instrum.* **26**, 1150–1157 (1955)
47. Okumura, M., Yeh, L.I., Myers, J.D., Lee, Y.T.: Infrared-spectra of the solvated hydronium ion - vibrational predissociation spectroscopy of mass-selected H₃O⁺·(H₂O)_N(H₂)M. *J. Phys. Chem.* **94**, 3416–3427 (1990)
48. Okumura, M., Yeh, L.I., Lee, Y.T.: Infrared-spectroscopy of the cluster ions H₃⁺·(H₂)_N. *J. Chem. Phys.* **88**, 79–91 (1988)
49. Okumura, M., Yeh, L.I., Myers, J.D., Lee, Y.T.: Infrared-spectra of the cluster ions H₇O₃⁺·H₂ and H₉O₄⁺·H₂. *J. Chem. Phys.* **85**, 2328–2329 (1986)
50. Kamrath, M.Z., Relph, R.A., Guasco, T.L., Leavitt, C.M., Johnson, M.A.: Vibrational predissociation spectroscopy of the H-2-tagged mono- and dicarboxylate anions of dodecanedioic acid. *Int. J. Mass Spectrom.* **300**, 91–98 (2011)
51. Leavitt, C.M., Wolk, A.B., Kamrath, M.Z., Garand, E., Van Stipdonk, M.J., Johnson, M.A.: Characterizing the intramolecular H-bond and secondary structure in methylated GlyGlyH⁽⁺⁾ with H-2 predissociation spectroscopy. *J. Am. Soc. Mass Spectrom.* **22**, 1941–1952 (2011)
52. Kamrath, M.Z., Garand, E., Jordan, P.A., Leavitt, C.M., Wolk, A.B., Van Stipdonk, M.J., Miller, S.J., Johnson, M.A.: Vibrational characterization of simple peptides using cryogenic infrared photodissociation of H-2-tagged, mass-selected ions. *J. Am. Chem. Soc.* **133**, 6440–6448 (2011)
53. Ufimtsev, I.S., Martinez, T.J.: Quantum chemistry on graphical processing units. 3. analytical energy gradients, geometry optimization, and first principles molecular dynamics. *J. Chem. Theory Comput.* **5**, 2619–2628 (2009)
54. Ufimtsev, I.S., Martinez, T.J.: Quantum chemistry on graphical processing units. 2. Direct self-consistent-field implementation. *J. Chem. Theory Comput.* **5**, 1004–1015 (2009)
55. Ufimtsev, I.S., Martinez, T.J.: Quantum chemistry on graphical processing units. 3. Analytical energy gradients and first principle molecular dynamics. *J. Chem. Theory Comput.* **5**, 2619 (2009)
56. Becke, A.D.: Density-functional exchange-energy approximation with correct asymptotic behavior. *Phys. Rev. A* **38**, 3098–3100 (1988)
57. Becke, A.D.: Density-functional thermochemistry. IV. A new dynamical correlation functional and implications for exact-exchange mixing. *J. Chem. Phys.* **104**, 1040–1046 (1996)
58. Lee, C., Yang, W., Parr, R.G.: Development of the Colle-Salvetti correlation-energy formula into a functional of the electron density. *Phys. Rev. B* **37**, 785–789 (1988)
59. Hehre, W.J., Ditchfield, R., Pople, J.A.: Self-consistent molecular orbital methods. XII. Further extensions of gaussian-type basis sets for use in molecular orbital studies of organic molecules. *J. Chem. Phys.* **56**, 2257–2261 (1972)
60. Frisch, M.J., Trucks, G.W., Schlegel, H.B., Scuseria, G.E., Robb, M.A., Cheeseman, J.R., Scalmani, G., Barone, V., Mennucci, B., Petersson, G.A., Nakatsuji, H., Caricato, M., Li, X., Hratchian, H.P., Izmaylov, A.F., Bloino, J., Zheng, G., Sonnenberg, J.L., Hada, M., Ehara, M., Toyota, K., Fukuda, R., Hasegawa, J., Ishida, M., Nakajima, T., Honda, Y., Kitao, O., Nakai, H., Vreven, T., Montgomery Jr., J.A., Peralta, J.E., Ogliaro, F., Bearpark, M.J., Heyd, J., Brothers, E.N., Kudin, K.N., Staroverov, V.N., Kobayashi, R., Normand, J., Raghavachari, K., Rendell, A.P., Burant, J.C., Iyengar, S.S., Tomasi, J., Cossi, M., Rega, N., Millam, N.J., Klene, M., Knox, J.E., Cross, J.B., Bakken, V., Adamo, C., Jaramillo, J., Gomperts, R., Stratmann, R.E., Yazyev, O., Austin, A.J., Cammi, R., Pomelli, C., Ochterski, J.W., Martin, R.L., Morokuma, K., Zakrzewski, V.G., Voth, G.A., Salvador, P., Dannenberg, J.J., Dapprich, S., Daniels, A.D., Farkas, Ö., Foresman, J.B., Ortiz, J.V., Cioslowski, J., Fox, D.J.: *Gaussian 09*. Gaussian, Inc., Wallingford, CT (2009)
61. Mesleh, M.F., Hunter, J.M., Shvartsburg, A.A., Schatz, G.C., Jarrold, M.F.: Structural information from ion mobility measurements: effects of the long-range potential. *J. Phys. Chem.* **100**, 16082–16086 (1996)
62. Shvartsburg, A.A., Jarrold, M.F.: An exact hard-spheres scattering model for the mobilities of polyatomic ions. *Chem. Phys. Lett.* **261**, 86–91 (1996)
63. Stearns, J.A., Seaiy, C., Boyarkin, O.V., Rizzo, T.R.: Spectroscopy and conformational preferences of gas-phase helices. *Phys. Chem. Chem. Phys.* **11**, 125–132 (2009)

64. Leavitt, C.M., Wolk, A.B., Fournier, J.A., Kamrath, M.Z., Garand, E., Van Stipdonk, M.J., Johnson, M.A.: Isomer-specific IR-IR double resonance spectroscopy of D-2-tagged protonated dipeptides prepared in a cryogenic ion trap. *J. Phys. Chem. Lett.* **3**, 1099–1105 (2012)
65. Siu, C.K., Guo, Y.Z., Saminathan, I.S., Hopkinson, A.C., Siu, K.W.M.: Optimization of parameters used in algorithms of ion-mobility calculation for conformational analyses. *J. Phys. Chem. B* **114**, 1204–1212 (2010)
66. Shi, L., Holliday, A.E., Shi, H., Zhu, F., Ewing, M.A., Russell, D.H., Clemmer, D.E.: Characterizing intermediates along the transition from polyproline I to polyproline II using ion mobility spectrometry-mass spectrometry. *J. Am. Chem. Soc.* **136**, 12702–12711 (2014)